PCCP

PAPER

View Article Online
View Journal | View Issue

Cite this: *Phys. Chem. Chem. Phys.*, 2014, **16**, 3534

Single bubble perturbation in cavitation proximity of solid glass: hot spot *versus* distance†

Darya Radziuk,[ab] Helmuth Möhwald[b] and Kenneth Suslick*[a]

Received 8th July 2013,
Accepted 20th August 2013

DOI: 10.1039/c3cp52850b

www.rsc.org/pccp

A systematic study of the energy loss of a cavitation bubble in a close proximity of a glass surface is introduced for the first time in a low acoustic field (1.2–2.4 bar). Single bubble sonoluminescence (SBSL) is used as a tool to predict the temperature and pressure decrease of bubble (μm) *versus* surface distance. A glass as a model system is used to imitate the boundary conditions relevant for nano- or micromaterials. SBSL preequilibrated with 5% argon is perturbed by a glass rod with the tip (Z-perturbation) and with the long axis (X-perturbation) at a defined distance. From 2 mm to 500 μm argon-SBSL lines monotonically narrow and the effective emission temperature decreases from 9000 K to 6800 K comparable to multiple bubbles. The electron density decreases by two orders of magnitude in Z-perturbation and is by a factor of two higher in X-perturbation than the unperturbed cavitating bubble. The perturbed single bubble sonoluminescence pressure decreases from 2700 atm to 1200 atm at 2.4 bar. In water new non-SBSL SiO molecular emission lines are observed and OH emission disappears.

1. Introduction

In nanotechnology acoustic cavitation is increasingly widespread as a simple and cheap technique to transform the surface energy into chemical, mechanical or thermal energy from the microscale down to the nanometers. In the liquid systems cavitation bubbles have been employed as extreme hot micro-reactors in otherwise cold bulk to fabricate novel nanomaterials,[1] functionalize with catalytic,[2] optical[3] and magnetic[4] properties for biological[5] and medical[6] purposes using a green ultrasonic approach. Although the nanostructuring is successful the advanced research requires the prediction of bubble conditions. In the liquid bulk solutions bubble formation, growth and collapse are unpredictable and the energy of cavitation is randomly averaged over multiple events.

The energy of the acoustic pressure field is focused locally by eleven orders of magnitude per molecule, atom or ion when compared to the energy of an emitted blue photon.[7] Molecular dynamics simulations predict that the peak temperatures can approach 10^8 K with duration of a few hundred femtoseconds.[8] There is no doubt in spectral evidence for the plasma existence inside the imploding bubbles.[9,10] To our knowledge the nature of plasma in acoustic bubbles is one of the key fundamental questions in acoustic cavitation,[11] energy,[12] nanotechnology and materials science[13] as well as biological imaging and medical diagnostics.[14,15]

Since the discovery of sonoluminescence (SL) from multiple bubbles[16] and later single bubble sonoluminescence (SBSL)[17] many research efforts have been concentrated to use SL as a thermometry tool to probe the bubble interior and to find out the origin of hot spots and their supersonic extremes.[11,18,19] To note in a conventional multi-bubble system SL arises inside the bubble at the end of the collapse and is emission from molecular, atomic or ionic species at excited states including radiative plasma processes. In contrast, SBSL requires a resonant standing ultrasound field and originates as a hot spot from a gas or a vapor filled micro bubble at the pressure antinode and comes in repetitive bursts.[20,21] The SBSL is rich in distinct emission bands of molecules, atoms and ions at excited states in low vapour pressure liquids and is spectrally poor in water.[22,23] In water SL spectra show a continuum background with a broad maximum reaching towards blue (300–400 nm) that is ascribed to OH bands[24] during water sonolysis. Although the spectra have poor resolution, the broad continuum can be well fitted to the blackbody curve at a temperature of 11 000 K with argon or

[a] *University of Illinois at Urbana-Champaign, Department of Chemistry (Chemical and Life Science Building), 600 S. Mathews Av., Urbana, IL 61801, USA. E-mail: radziuk@illinois.edu, ksuslick@illinois.edu; Fax: +1 217-244-3186; Tel: +1 217-333-1532*

[b] *Max-Planck Institute of Colloids and Interfaces, Department of Interfaces, Am Mühlenberg 1, D14476 Potsdam (Science Campus Golm), Germany. E-mail: darya.radziuk@mpikg.mpg.de, helmuth.moehwald@mpikg.mpg.de; Fax: +49 (0)331-567-9202; Tel: +49 (0)331-567-9447*

† Electronic supplementary information (ESI) available: The sketch of the experimental set-up, single bubble sonoluminescence (SBSL) spectra during X-perturbation, the isolated SBSL Ar atom 763.51 nm emission line of a high resolution during Z-perturbation, average normalized deviation (%) of SBSL Ar atom emission spectra from best fits to a Lorentzian function, the spectral radiant power of SBSL perturbed by a glass surface with 5% Ar in aqueous solution of 85 wt% H_2SO_4 or in deionized ultrapure water without perturbation, and with air during X-perturbation by a glass rod are shown in Fig. SI 1–SI 7, Tables S1 and S2. See DOI: 10.1039/c3cp52850b

helium, whereas 8000 K resembles similar for oxygen or nitrogen. A pressure of 5×10^3 atm at 10^4 K of the hot gas phase interior was estimated for the first time by calculating the half widths of D sodium emission lines.[25]

Various approaches based on SL spectral observation were developed to find out the temperature and pressure of cavitation,[26,27] its energy efficiency[28] and prove the plasma existence.[29] Common liquid bulk solutions for SL studies contained dissolved noble gases or air. Earlier SL liquids used water with a noble gas and electrolytes,[30–32] long-chain hydrocarbons and silicone oils,[33,34] and later ionic liquids[35] and aqueous electrolytic solutions such as mineral acids (*i.e.* $HClO_4$, H_2SO_4),[29] and recently H_3PO_4.[23] The choice of the nonaqueous SL solutions was controlled by the low vapor pressure at room temperature (*e.g.* 40 mTorr for 85 wt% H_2SO_4), their transparency in the spectral region from the UV to the near IR and high brightness. From the relative intensities of spectral lines the temperature of the gaseous phase can reach higher than 15 000 K. It is controlled by the acoustic intensity and the nature of a filling gas. The internal pressure of SBSL reaches values ranging from 3700 atm as it has been estimated using two independent methods.[27]

In recent years, an alternative approach to probe the bubble events from nucleation to the prediction of their growth was proposed by the study of cavitation near a solid surface with partially hydrophobic and hydrophilic patterns.[36] One could use solid surfaces as direct fingerprints of bubble events followed at the end by cavitation erosion, oxidation, damage (pit formation, amorphization, melting, *etc.*) and destruction including dissolution of interfacial layers. By calculation of surface defects one can estimate the nucleation energy and predict the bubble growth. However, it is difficult to get knowledge about the temperature and pressure from a bubble close to or at the surface and predict the shock wave or jet scenario.

Shock waves and jets are applied in many aspects of modern medicine and biology including diagnostics and therapeutics, membrane disrupture,[37] molecular imaging, drug and gene delivery therapies.[38–42] The symmetry of bubble collapse depends on its shape geometry: shock waves are mostly created in spherical bubbles, while jets are developed from the strong asymmetry towards the surface.[43] There is a key challenge in sonoporation, cell damage or membrane disruption to predict the energy distribution from a bubble in close proximity of a rigid biological boundary. In addition, the rate of surface deformation due to the interaction with a hot spot is unknown. The question to answer is what is the temperature or pressure delivered to the surface and at what distance.

On the other hand, the surface itself can be used as a perturber of a bubble and cause either the cooling or heating of its gaseous interior. Varying the distances towards the solid surface one could directly collect the SL spectrum and estimate the energy loss or gain from the cavitation bubble. Previously, the effect of perturbation on SBSL was limited by a bubble's hemispherical shape with insignificant differences in neither dynamics nor featureless spectra.[44] No pressure or plasma conditions were quantified and the hot spot conditions were unclear. However, the decrease of SBSL continuum closer to the surface showed the thermal cooling of a bubble with a random blackbody temperature of 7400 K.[45] However, systematic calculation of temperature *versus* surface distance was impossible due to the absence of distinct spectral lines. To note, a noisy underlying continuum could be only fitted to the classical blackbody model and accurate spectral methods (*e.g.* plasma diagnostics) cannot be applied. Moreover, this study was unable to find out the changes in the bubble pressure delivered to the surface *versus* distance.

In the present work, single bubble sonoluminescence is used as a tool to systematically estimate the energy loss of the cavitation bubble approaching the glass surface at distances from 1 cm to 500 mm. Distinct from previous studies,[46,47] SBSL with argon was formed in water or aqueous solution of sulfuric acid and collected at a low acoustic field (1.2–2.4 bar). A glass rod perturbed SBSL by approaching with a tip (Z-perturbation) or with a long side (X-perturbation). Applying the plasma diagnostics method to the argon atom SBSL spectral lines we plotted the effective emission temperature and pressure loss of the bubble *versus* surface distance. It is remarkable that the electron density, ionization degree and ion broadening parameters could also be derived closer to the glass surface. This challenging work elegantly shows not only the bubble energy distribution in the close proximity of a surface, but also new excitation pathways to observe non-SBSL SiO emission from glass in water.

2. Experimental section

2.1. Materials

Sulfuric acid (98% H_2SO_4, Merck Millipore, USA), ultrapure water (>18 MΩ cm, Thermo Scientific Barnstead Nanopure, USA), Ar (99.999% purity, Matheson Gas Products, Secaucus, NJ), the piezoceramic element (PZT, Channel Industries, USA) were used in experiments.

2.1.1. Preparation of sulfuric acid solutions for single bubble sonoluminescence

The experimental set-up for perturbation of SBSL near a glass surface is shown in Fig. SI 1 (ESI†). Typically 112 mL of solution was prepared by dilution of 95–98% H_2SO_4 (98% Merck Millipore, USA) to 85 wt% with ultrapure water (18 MΩ cm, Thermo Scientific Barnstead Nanopure, USA). Degassing was carried out under vacuum (<0.1 Torr) with stirring at 23 °C for 24 hours. The solution was regassed with Ar (99.999% purity, Matheson Gas Products, Secaucus, NJ) for 1 hour in a closed system.

2.1.2. Measurements of single bubble sonoluminescence perturbation in sulfuric acid solution

A single bubble was formed in the center of a spherical quartz resonator (diameter 60 mm) and driven at ~30 kHz frequency by the piezoceramic element (PZT, Channel Industries, USA) on the bottom. A piezoceramic pill microphone with smaller size was glued on the outer wall of the SBSL resonator in order to monitor the quality of the resonance. The 1000 Q factor of the quartz resonator was determined by triggering the oscilloscope

with 5000 burst cycles at 2 Hz frequency under resonant conditions. This Q factor is relatively high and means a long ring time since no other mode takes energy from the main resonance after the driving signal is turned off. The shape profile and amplitude of the ultrasound wave were monitored in real time using a digital oscilloscope (Tektronix TDS 3052 two channel color digital phosphor oscilloscope 500 MHz) and controlled using a function generator (Hewlett Packard 33120A, 15 MHz) and an amplifier (research model 700-A1, 700 Watt).

The perturbation distance from 1.5 mm to 500 μm was mechanically controlled *via* the translation stage mounted to the quartz resonator cell. At a length shorter than 0.5 mm the counteraction of Bjerknes and buoyancy forces violates the stability of levitation, and the bubble disappears. For optimal brightness the SB reaction solution was carefully degassed under vacuum to eliminate air and avoid the natural quenching.[6] Degassing was followed by regassing with argon at a low partial pressure (38–40 Torr) to achieve optimal spatial stability and singularity of the single bubble and a relatively high signal to noise ratio for the spectra acquisition. At partial concentration of argon below 5% the SBSL was dim and hardly visible by the naked eye with poor atomic emission lines disabling spectral analysis. In contrast, at partial pressures of argon increased by a factor of 3, the SBSL was very bright but the reaction solution became too gassy with highly unstable bubbles due to excess of nucleation points.

The SBSL spectra were collected with 300 g mm^{-1} blazed at 250 nm or 1200 g mm^{-1} blazed at 330 and 750 nm and recorded using a spectrograph (TRIAX 320 Jobin Yvon-SPEX Instruments S.A., Inc.) with the CCD-3000 camera. The visible range of the electromagnetic spectra was filtered with the cut off at 300 nm in order to avoid the second order emission at longer wavelengths. The signal to noise ratio was high enough to ensure the low value of the root mean square fluctuations averaged in time (typically below 5%).

All spectra were corrected for absorption by solution and the resonator and for the response to the optical system. The spectral radiance was performed with NIST-F-211-traceble standards of known spectral irradiance (The Eppley Laboratory Inc., Eplab scientific instruments).[36] The calibrated deuterium lamp and a quartz tungsten halogen lamp with neutral density filters are well within the known limits of accuracy. A needle hydrophone (Dapco Industries, model NP-10-1) was used to measure the acoustic pressure field. SBSL was driven at low acoustic pressure amplitudes to maintain the bubble spatial stability that is achieved in the counteraction of buoyancy and Bjerknes forces.

2.1.3. Measurements of single bubble sonoluminescence perturbation in water

Deionized ultrapure water (>18 MΩ cm) was degassed to <24 mbar pressure for 45 min and regassed with Ar ($\sim 5\%$) during another 30 min under stirring. A SBSL was formed in a quartz resonator cell with cylindrical geometry (height 9 cm, inner diameter 5.2 cm, volume 180 mL).[54] A solitary bubble was driven at 27 kHz ultrasound frequency controlled using a wideband power amplifier (Krohn-Hite model 7500) and a linear sweep function generator (Linear Krohn-Hite, model 1200A). The driving acoustic pressure was measured using a needle hydrophone (Dapco Industries, model NP-10-1) connected to an oscilloscope (HAMEG, HM407, SP107).

All spectra were collected with a 600 g mm^{-1} blazed at 300 nm or 300 g mm^{-1} blazed at 500 nm gratings with 100 s or 300 s total acquisition time. A triplet lens system (Edmund Optics) was placed on the entrance slit of 100 μm width of an Acton Research SP-300i imaging spectrometer with a charge-coupled-device detector (PIXIS 100B, Princeton Instrument). In the visible range the long pass filter at 320 nm was used.

2.1.4. Determination of the effective SBSL temperature

The two radiance line ratio method was applied to determine the effective SBSL temperature, T_{eff}, as it removes the need to know the path length and number density. The T_{eff} emission temperature is calculated from the relative intensities of two argon atom emission spectral lines of transitions from different excited states that are separated in energy

$$\frac{I_1}{I_2} = \frac{g_1 A_1 \lambda_2}{g_2 A_2 \lambda_1} \exp[(E_2 - E_1)/kT_{\mathrm{eff}}] \quad (1)$$

where I_1, I_2 are the relative intensities of Ar atom emission lines from 4p–4s manifold (13.5–11.5 eV), g, A, λ, E are constants of the degeneracy of the state, the Einstein transition probability, the light wavelength and the energy of the state for Ar atom emission lines, respectively.[29] Among 20 SBSL Ar atom emission lines that are present from 690 to 900 nm only 6 are intense enough and well isolated. The selected lines for the T_{eff} determination are 696 nm, 706 nm, 738 nm, 763 nm, 794 nm and 826 nm. The requirement is that the SBSL follows a Maxwell–Boltzmann distribution so that the average kinetic energy of an atom or a molecule is directly proportional to the absolute temperature multiplied by 3/2 and the Boltzmann constant k. The densities of atomic species are in local thermodynamic equilibrium. The emitting radius of SBSL is in the order of the light wavelength, and correction for self-absorption is not undertaken. The effective gas temperature is determined by measuring the relative populations of two or more states with a relative accuracy below 5% reported elsewhere.[37]

The measured temperature is considered to be an effective characteristic of the atoms concerned and not necessarily of the free electrons or ions in the plasma. The limitation of this method is not critical for our calculation since this method becomes insensitive and inaccurate for high temperature plasmas due to small energy differences compared to kT for the lines of a common species. Correction to the ionization potential is introduced due to the Coulomb interactions, which is true for local thermodynamic equilibrium. Bremsstrahlung can be excluded as it requires the presence of unbound electrons (substantial ionization) and T in the order of 10^6–10^7 K and is true for high gas densities.[38]

2.1.5. Determination of the ion broadening parameter, ionization degree and electron density

In general line asymmetry depends on the relative importance of heavy-ion broadening to electron broadening and this is

described by a dimensionless parameter designated as '*A*'. An *A* value shows deviation of the asymmetrically ion-broadened line from a symmetric Lorentzian profile. The isolated 763 nm SBSL Ar atom emission band profile was fitted to a Lorentzian function and the standard deviation of the individual line from a Lorentzian least-square-fit was calculated, normalized *versus* the peak centre offset in FWHM (Fig. SI 5, ESI†). The shape of the deviation curve is independent of the emitting element. This allows one to determine the critical intracavity plasma properties as ion broadening parameter (A), degree of ionization (α) and electron density (N_e, cm^{-3}). An A value was determined by analyzing the amplitude of the first negative deviation of the asymmetrically broadened line from a symmetric dispersion-type line. The amplitude at minimum of this deviation, Δ_{min}, gives the estimation of the A value, which scales by a 4/3 power with the degree of ionization (α) and a $\frac{1}{4}$ power with the electron density (N_e, cm^{-3}). The degree of ionization was determined by direct comparison of the previously measured number density of neutral Ar atoms to the free electron density.[6]

The other dimensionless parameter which the line asymmetry depends on is the Debye shielding parameter designated as R and reflects the shielding of heavy-ion perturbation by plasma electrons. Basically R shows the ratio of the mean ion–ion separation to the Debye radius and is determined as,

$$R = \sqrt[6]{\frac{36\pi e^6 N_e}{(k_B T)^3}}$$

Where e is the elementary charge (1.6×10^{-19} Coulomb), $k_B T$ is Boltzmann's constant multiplied by the temperature and N_e is the electron density. For our calculations we used $R = 0.55$ in all fitting since the resulting A values are relatively insensitive to this Debye shielding parameter. The accuracy of these estimations is limited by experimental errors in the intensity ratio and the electron densities up to 10% for values higher than 10^{18}. For lower N_e values uncertainties in the equilibrium relations make the temperature estimate much less certain, therefore the accepted error for electron density calculation is about 18%.

2.1.6. Calculation of SBSL pressure

From the classical trajectory theory we can determine the reduced mass of the collision partners as

$$\mu = \frac{m_A m_{BC}}{m_A + m_{BC}} \cdot \frac{1\ \text{kg}}{1000\ \text{g}} \cdot \frac{1\ \text{mol}}{\text{Na}}$$

considering Ar atoms only,

$$m_A = m_{Ar},\ m_{BC} = m_{Ar}$$

$$\mu_{Ar} = \frac{m_{Ar}}{2} \cdot \frac{1\ \text{kg}}{1000\ \text{g}} \cdot \frac{1\ \text{mol}}{\text{Na}}$$

and,

$$\mu_{Ar} = \frac{M}{2\text{Na}} = 3.3 \times 10^{-23}\ \text{g}$$

the density within the observed emitting region is,

$$n_{Ar} = \frac{\text{FWHM}}{\sqrt{\frac{8k_B T_c}{\pi^3 \mu_{Ar}} \cdot \pi (2r_{Ar})^2}}$$

Where FWHM is the Full Width at Half Maximum (from the best Lorentzian fit), k_B is the Boltzmann's constant, T_c is the critical temperature (calculated for the Ar atom emission line), μ_{Ar} is the reduced mass of the collision Ar atoms and is the distance between the centers of two Ar atoms with the Ar van der Waals radius r_{Ar} each being 188 pm.

The effective local density during cavitation is determined as

$$P_c = \frac{3RT_c}{8n_{Ar}}$$

and the pressure of SBSL is

$$P_{SBSL} = \frac{RT_c n_{Ar}}{\text{Na}}$$

assuming ideal gas state conditions. The relative error of SBSL pressure estimation is less than 5%.

3. Results and discussion

SBSL is perturbed by a glass rod approaching with a tip (Z-perturbation) (Fig. 1A) or with a long side (X-perturbation) (Fig. 1B) in the house made quartz spherical resonator mounted to a XYZ translation stage (Fig. SI 1, ESI†).

Two different liquids with argon are compared: 85 wt% H_2SO_4 and ultrapure water. In sulfuric acid the effect of perturbation on the SBSL is examined using the spectral band profiles of Ar atom emission lines. In water the observation of new spectral lines during SBSL perturbation is in the focus. Glass as a perturbation substance can serve as a model boundary for a bubble cavitating near soft bio-materials or substrates relevant for biophysical application.

In the range of acoustic pressure below 2.4 bar SBSL acquires a steady state oscillation in Z-perturbation (Fig. 1A). Closer to

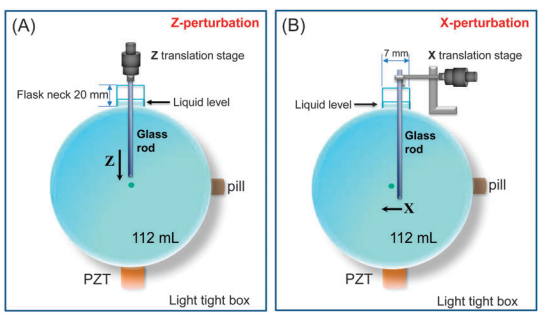

Fig. 1 Sketch of the spherical resonator for SBSL perturbation by a glass rod (diameter 1 mm) in 85 wt% H_2SO_4 regassed with 5% Ar, (A) in Z-perturbation of a SBSL the glass rod approaches the bubble with the tip along the vertical Z axis. (B) X-perturbation of a SBSL occurs along the horizontal X axis; the glass rod is fixed to the X translation stage on the top of the flask neck and approaches the bubble in direction X normal to the rod direction Z.

the glass surface the SBSL undergoes translational motion away from the rod directed to the bottom of the resonator. In a higher pressure field at 2.7 or 3.1 bar the translational motion of SBSL transformed into shape of an "eight" or a "circle" in the mm range. Similar dynamics of SBSL was observed in acoustic fields of 5 bar and the shape of SBSL traces acquired larger "circles" or "ellipses" (<5 mm).[48] Note that at high acoustic intensities the relative diameter ratio of the SBSL translational profile did not increase. Moreover, no steady state oscillations were observed in the range from 2.4 bar to 3.1 bar during X-perturbation (Fig. 1B). It is remarkable that the perturbation of SBSL was limited to 3.1 bar acoustic pressure since the bubble stability is strongly decreased and further collection of SBSL spectra was technically difficult.

Typically the unperturbed SBSL shows a featureless continuum in the UV region and Ar atom emission lines on the top of the decayed continuum in the near IR. The UV part of the emission spectrum is very intense and independent of the atomic species described by Planck's law. From the blackbody fit the temperature of the SBSL continuum is 9000 K at 2.3 bar.[9] This is comparable to SBSL Ar lines at 2.9 bar in the near IR region when the bubble is at 1.5 mm from the glass rod (Fig. 2). The effective emission temperature of Ar-SBSL decreases from 9300 K to 6800 K when the glass rod approaches the bubble to 500 μm the closest distance.

At acoustic intensity equivalent to 2.4 bar the SBSL shows strong SBSL Ar lines at 738 nm, 750 nm, 763 nm and 772 nm due to the 4p–4s manifold (13.5 eV–11.5 eV) (Fig. SI 2, ESI†). The small emission peak near 777 nm is assigned to oxygen atom emission from the 3p (10.7 eV) and 3s (9.15 eV) manifold.[49,50] At distances 1 mm and 0.9 mm from the glass rod along Z the narrowing of Ar lines is indistinguishable. Closer to the glass surface monotonic asymmetry gradually developed along the wings of the spectral lines.

Fig. 3 shows the decrease of the effective SBSL temperature, T_{eff}, *versus* perturbation distance by a glass rod.

The upper temperature range of similar SBSL (Table S1, ESI†) is consistent with previous studies.[9] Although all single

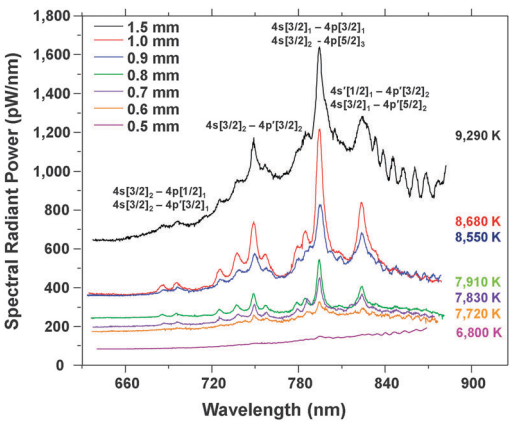

Fig. 2 X-perturbation of SBSL spectra in 85 wt% H_2SO_4 with 7% Ar at 2.9 bar acoustic pressure field. The spectra were collected with a grating 300 g mm^{-1} blazed at 250 nm at 100 μm slit width.

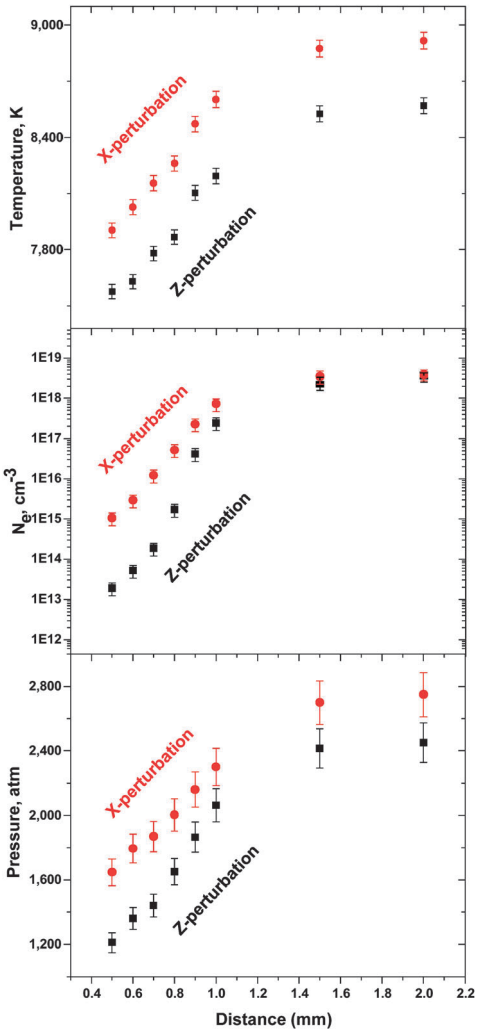

Fig. 3 Effective temperature T_{eff} (K), electron density N_e (cm^{-3}) and pressure P_{SBSL} (atm) of SBSL *versus* perturbation distance (mm) from the glass rod in 85 wt% H_2SO_4 regassed with Ar at acoustic intensity equivalent to 2.4 bar.

sonoluminescing bubbles were created in identical solutions and measurements were repeated at least ten times for each event, still there is a slight difference of T_{eff} and P_{SBSL} at distances above the perturbation region. The temperature gradient is higher during Z-perturbation than it is in X-perturbation. Without perturbation in the range of driving P_{ac} from 1.2 bar to 2.4 bar the gradient of the SBSL T_{eff} is comparable to X-perturbation (Table S2, ESI†).

The isolated 763 nm SBSL Ar line narrows monotonically without a pronounced peak shift but with a slight asymmetry (Fig. 4) consistent with long-range Coulomb interactions.

In X-perturbation the gradual FWHM (full width at half maximum) decay from 1 mm to 0.5 mm occurs stronger in the red wavelength region. At the distance from 2 mm to 1.5 mm SBSL is unperturbed (Table S1, ESI†). In Z-perturbation the SBSL FWHM decreases asymmetrically, but less monotonic (Fig. SI 3, ESI†). The narrowing of the perturbed SBSL Ar line shows the decreased rate of interaction between radiating and neutral

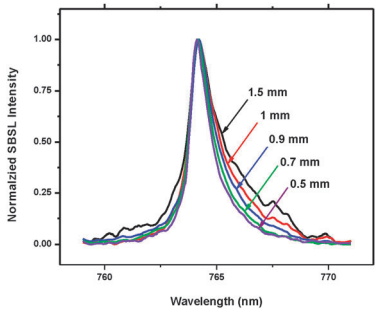

Fig. 4 Isolated 763 nm SBSL Ar atom emission lines during perturbation from 1.5 mm to 0.5 mm by a glass rod aligned along *Z* and approaching along *X*. These spectra were collected with high resolution grating 1200 g mm^{-1} blazed at 750 nm and 100 μm slit width and smoothed using the gentle Savitzky–Golay method (5 points of window).

atoms with charged species (*i.e.* ions or electrons).[50] From Stark theory these collisions act separately and uncorrelated in time since Ar atoms are heavy particles with the relatively slow movement.

In general line asymmetry depends on the relative importance of heavy-ion broadening to electron broadening and this is described by a dimensionless parameter designated as '*A*'.[50,51] An '*A*' value shows deviation of the asymmetrically ion-broadened line from a symmetric Lorentzian profile and its value can be estimated from the amplitude at minimum of this deviation, Δ_{min} (Fig. SI 4, ESI†). In Z-perturbation the decrease of the ion broadening parameter is higher than it is in X-perturbation (Table S1, ESI†) comparable to unperturbed curves at P_{ac} from 1.2 bar to 2.4 bar (Table S2, ESI†).

The ionization of SBSL Ar atoms occurs at low ionization degree, α, (Tables S1 and S2, ESI†) due to the fact that the statistical weight of the free states of electrons is very broad. The α value decreases from 10^{-5} to 10^{-6} closer to the glass surface and has a higher decay rate than unperturbed SBSL (Table S1, ESI†). It is consistent with the previous study assuming a much lower driving pressure.[46] The α value is higher in Z-perturbed Ar-SBSL and shows a slightly higher number of ionized atoms. Although Ar is considered to be a heavy gas, a continuous sequence of multiple ionization is excluded as the SBSL T_{eff} is less than tens of thousands K.

The N_e of SBSL decreases by two orders of magnitude faster during Z-perturbation (Fig. 3 and Table S1, ESI†) and by a factor of three higher in X-perturbation compared to the unperturbed Ar-SBSL at low acoustic intensity (Table S2, ESI†). The Ar-SBSL pressure decreases at a faster rate in Z-perturbation and slower in X-perturbation (Fig. 3, Table S1, ESI†) comparable to the unperturbed Ar-SBSL (Table S2, ESI†). In SBSL the stronger decay of SBSL pressure is associated with the decreased number of particle collisions and a cooling of low density plasma. This might explain the stronger difference of N_e decay during Z-perturbation. Moreover, the Z-perturbation has a cylindrical symmetry, for large distance is 2-dimensional but at the closest approach it looks like a plane. X-perturbation is 1-dimensional line distortion, but the symmetry has a plane of reflection. It may be less effective, because the average distance from the bubble is shorter.

At the shortest X-perturbation distance the SO molecular emission is observed on the top of the SO_2 quasicontinuum (Fig. SI 5, ESI†). Similar fluorescence spectra were observed during electron impact on SO_2.[52,53] The relatively low kinetic energy of electrons (8–18 eV) is in agreement with the ionization degree of perturbed SBSL (Table S1, ESI†). Many of the O I, O II, S I and S II features below 26 000 cm^{-1} are not observed since the electron incident energy for the additional excitation processes lies at 98 eV. At high wavenumbers SO_2 accesses more dissociative and ionization states and SO emission of 10.4 eV is observed. The temperature of the SO SBSL is about 2100 K as estimated recently in neon bubbles.[54] On the top of the continuum two small peaks at 349 and 357 nm can be assigned to Ar^+ emission due to the 4p–4s array transition (37.1–32.4 eV).[55] This is fully consistent with the previous observation[29] and proves the plasma[10] formation during perturbed SBSL. Note, no O_2^+ emission was observed probably due to the low ionization degree, so that electrons have insufficient kinetic energy (< several hundred eV) for excitation of O_2^+.[56] No additional emission lines from the glass surface were observed under these conditions and also at P_{ac} = 1.9 bar–1.5 bar, at 2.7 bar and 3.1 bar or 3%, 8%, 10% and 12% partial concentrations of Ar.

In water (5% Ar) the bubble translational motion has a higher speed due to the 25 times lower viscosity (at RT) and the 1.25 times higher expansion ratio[57] than in 85% sulfuric acid solution. Water molecules dissociate and hydroxyl-radicals emit light during recombination of $H^\bullet$ and $OH^\bullet$ species and deactivation of excited OH species[58] (Fig. SI 6, ESI†). Unperturbed Ar-SBSL shows OH ($A^2\Sigma^+ - X^2\Pi$) emission that is assigned to the main Q-branch K → K free molecule dipole transitions. The vibrational structure is introduced by a strong peak at 308 nm due to the (ν', ν'') = (0, 0) transition with the main head Q_2 and by its high frequency shoulder at 288 nm (ν', ν'') = (2, 1) with the Q_1 head.[24]

In X-perturbed Ar-SBSL in water new emission lines are observed from 250 nm to 450 nm and can be assigned to SiO molecular emission[24] (Fig. 5).

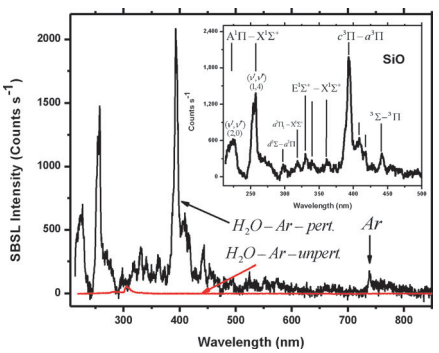

Fig. 5 SBSL spectra with 5% Ar in deionized ultrapure water (18 MΩ cm) during X-perturbation by a glass rod. The spectra were collected at applied acoustic pressure of 1.17 bar at 19 °C with the average acquisition time 100 s (600 g mm^{-1} blazed at 300 nm grating and 250 μm slit width). The black arrow shows the emission spectra during perturbation designated as "H_2O-Ar-pert." and a red arrow points at an unperturbed SBSL spectrum in a red color ("H_2O-Ar-unpert."). The inset shows the magnified UV region of "H_2O-Ar-pert." with the assignment to the SiO molecular emission lines.

Two strong single-headed peaks at 258 nm are due to the $A^1\Pi - X^1\Sigma^+$ transition and a triple-headed one at 393 nm is due to the $c^3\Pi - a^3\Pi$ transition. Both peaks are red broadened with the highest intensity among the many other small emission lines at 297 nm ($d^3\Sigma - a^3\Pi$); 320 nm ($d^3\Sigma - a^3\Pi$); 320 nm ($a^3\Pi_1 - X^1\Sigma^+$); 330, 341 and 361 ($E^1\Sigma^+ - X^1\Sigma^+$) and at 441 ($^3\Sigma - {}^3\Pi$) (inset in Fig. 5). In the near IR the perturbed SBSL shows a small peak from Ar atom emission at 740 nm (Fig. 5). Note, no SiO emission was detected in air containing water, and the SBSL spectrum showed a broad band in the UV region similar to that without perturbation (Fig. SI 7, ESI†).

The SiO emission can occur from the population of excited electronic states by means of radiationless transitions induced by high pressures near cracks or local fractured areas.[59] The surface fracture of glasses was also observed in multiple bubbles but without SiO emission.[60] The SiO emission may occur due to the possible mechanisms:

– Shock wave and high pressure impact after bubble collapse;

– Jets creating the surface defects on the glass surface;

– Interparticle collisions between silica particles removed from the glass surface during fracturing.

4. Conclusions

In conclusion, the perturbation of Ar-SBSL by a glass rod causes monotonic thermal cooling of a hot spot. At a closest experimentally achievable distance (500 μm), the single bubble remains hot (~6800 K), comparable to multiple bubbles. The electron density, N_e, decays by two orders of magnitude lower in X-perturbation, but by a factor of two higher than in unperturbed Ar-SBSL in a low acoustic pressure field (1.2–2.4 bar). As the Ar lines narrow the Ar-SBSL pressure decreases from 2700 atm to 1200 atm during perturbation. Z-perturbation is more effective than X-perturbation because it has a cylindrical symmetry and at longer distances acts as a 2-dimensional perturber. New SiO emission lines are in X-perturbed Ar-SBSL in water and OH emission disappears. Under similar conditions a small Ar^+ ion emission is observed in 85 wt% H_2SO_4: more proof for plasma.

The reported results can be of significant interest to scientific community and industry dealing with cavitation bubbles and its application in surface science, green energy chemistry, sonochemistry, nanotechnology, biology and medicine.

Acknowledgements

Financial support by the DFG and NSF CHE 1011972 grants is acknowledged. We thank Prof. David Flannigan for useful comments.

Notes and references

1 J. H. Bang and K. S. Suslick, *Adv. Mater.*, 2010, **22**, 1039.
2 G. Park, L. Bartolome, K. G. Lee, S. J. Lee, D. H. Kim and T. J. Park, *Nanoscale*, 2012, **4**, 3879.
3 D. Radziuk, A. Skirtach, A. Geßner, M. U. Kumke, W. Zhang, H. Mohwald and D. Shchukin, *Langmuir*, 2011, **27**, 14472.
4 D. Niu, X. Wang, Y. Li, Y. Zheng, F. Li, H. Chen, J. Gu, W. Zhao and J. Shi, *Adv. Mater.*, 2013, **25**, 2686.
5 U. Shimanovich, V. Volkov, D. Eliaz, A. Aizer, S. Michaeli and A. Gedanken, *Small*, 2011, **7**, 1068.
6 T. Yin, P. Wang, J. Li, R. Zheng, B. Zheng, D. Cheng, R. Li, J. Lai and X. Shuai, *Biomaterials*, 2013, **34**, 4532.
7 B. P. Barber and S. J. Putterman, *Nature*, 1991, **352**, 318.
8 A. Bass, S. J. Ruuth, C. Camara, B. Merriman and S. Putterman, *Phys. Rev. Lett.*, 2008, **101**, 234301(1).
9 D. J. Flannigan and K. S. Suslick, *Nature*, 2005, **434**, 53.
10 A. A. Ndiaye, R. Pflieger, B. Siboulet and S. I. Nikitenko, *Angew. Chem., Int. Ed.*, 2013, **52**, 2478.
11 K. S. Suslick and D. J. Flannigan, *Annu. Rev. Phys. Chem.*, 2008, **59**, 659.
12 M. C. Ramsey and R. W. Pitz, *Phys. Rev. Lett.*, 2013, **110**, 154301(1).
13 H. Xu, B. W. Zeiger and K. S. Suslick, *Chem. Soc. Rev.*, 2013, **42**, 2555.
14 L. Mail, A. Yaol, J. Li, Q. Wei, M. Yuchi, X. He, M. Ding and Q. Zhou, *PLoS One*, 2013, **8**, 1224(1).
15 Y. Negishi, N. Hamano, Y. Tsunoda, Y. Oda and B. Choijamts, *et al.*, *Biomaterials*, 2013, **34**, 501.
16 N. Marinesco and J. J. Trillat, *Proc. R. Acad. Sci.*, 1933, **196**, 858.
17 D. F. Gaitan, L. A. Crum, C. C. Church and R. A. Roy, *J. Acoust. Soc. Am.*, 1992, **91**, 3166.
18 S. J. Putterman and K. R. Weninger, *Annu. Rev. Fluid Mech.*, 2002, **34**, 445.
19 M. P. Brenner, S. Hilgenfeldt and D. Lohse, *Rev. Mod. Phys.*, 2002, **74**, 425.
20 D. F. Gaitan, L. A. Crum, C. C. Church and R. A. Roy, *J. Acoust. Soc. Am.*, 1992, **91**, 3166.
21 K. R. Weninger, B. P. Barber and S. J. Putterman, *Phys. Rev. Lett.*, 1997, **78**, 1799.
22 D. J. Flannigan and K. S. Suslick, *Phys. Rev. Lett.*, 2005, **95**, 044301(1).
23 H. Xu and K. S. Suslick, *Phys. Rev. Lett.*, 2010, **104**, 244301(1).
24 R. W. B. Pearse and A. G. Gaydon, *The Identification of Molecular Spectra*, John Wiley and Sons, Inc., New York, US, 4th edn, 1976.
25 S. Robin, J. Robin and B. Vodar, *C. R. Hebd. Seances Acad. Sci.*, 1951, **232**, 1754.
26 D. J. Flannigan and K. S. Suslick, *J. Phys. Chem. Lett.*, 2012, **3**, 2401.
27 D. J. Flannigan, S. D. Hopkins, C. G. Camara, S. J. Putterman and K. S. Suslick, *Phys. Rev. Lett.*, 2006, **96**, 204301.
28 Y. T. Didenko and K. S. Suslick, *Nature*, 2002, **418**, 394–397.
29 D. J. Flannigan and K. S. Suslick, *Phys. Rev. Lett.*, 2005, **95**, 044301(1).
30 F. R. Young, *J. Acoust. Soc. Am.*, 1976, **60**, 100.
31 M. Wall, M. Ashokkumar, R. Tronson and F. Grieser, *Ultrason. Sonochem.*, 1999, **6**, 7.
32 E. B. Flint and K. S. Suslick, *J. Phys. Chem.*, 1991, **95**, 1484.
33 K. S. Suslick and E. B. Flint, *Nature*, 1987, **330**, 553.

34 K. S. Suslick, E. B. Flint, M. W. Grinstaff and K. A. Kemper, *J. Phys. Chem.*, 1993, **97**, 3098.
35 P. M. Kanthale, A. Brotchie, F. Grieser and M. Ashokkumar, *Ultrason. Sonochem.*, 2013, **20**, 47.
36 V. Belova, D. A. Gorin, D. G. Shchukin and H. Mohwald, *Angew. Chem., Int. Ed.*, 2010, **49**, 7129.
37 P. Prentice, A. Cuschieri, A. Cuschieri, K. Dholakia, M. Prausnitz and P. Campbell, *Nat. Phys.*, 2005, **1**, 107.
38 H. Chen, A. A. Brayman, W. Kreider, R. M. Bailey and T. J. Matula, *Ultrasound Med. Biol.*, 2011, **37**, 2139.
39 M. Overvelde, V. Garbin, B. Dollet, N. De Jong, D. Lohse and M. Versluis, *Ultrasound Med. Biol.*, 2011, **37**, 1500.
40 S. W. Ohl, E. Klaseboer and B. C. Khoo, *J. Phys. Med. Biol.*, 2009, **54**, 6313.
41 R. Dijkink, S. Le Gac, E. Nijhuis, A. van den Berg, I. Vermes, A. Poot and C. D. Ohl, *J. Phys. Med. Biol.*, 2008, **53**, 375.
42 C. D. Ohl, M. Arora, R. Ikink, N. de Jong, M. Versluis, M. Delius and D. Lohse, *J. Biophys.*, 2006, **91**, 4285.
43 L. A. Crum, *J. Phys.*, 1979, **41**, 285.
44 K. R. Weninger, H. Cho, R. A. Hiller, S. J. Putterman and G. A. Williams, *Phys. Rev. E*, 1997, **56**, 6745.
45 E. A. Brujan and G. A. Williams, *Phys. Rev. E*, 2005, **72**, 016301.
46 D. J. Flannigan and K. S. Suslick, *Nat. Phys.*, 2010, **6**, 598.
47 J. B. Young, J. A. Nelson and W. Kang, *Phys. Rev. Lett.*, 2001, **86**, 2673.
48 D. J. Flannigan and K. S. Suslick, *J. Acoust. Res. Lett. Onl.*, 2005, **6**, 157.
49 G. Herzberg, *Molecular Spectra and Molecular Structure. Spectra of Diatomic Molecules*, Kriger Publishing Company, Malabar, Florida, US, 2nd edn, 1989, vol. I.
50 H. R. Griem, *Spectral Line Broadening by Plasmas*, Academic Press, New York, US, 1974.
51 V. Milosavljevic and S. Djenize, *J. Astron. Astrophys.*, 2003, **398**, 1179.
52 J. M. Ajello, G. K. James and I. Kanik, *J. Geophys. Res.*, 1992, **97**, 10501.
53 J. M. Ajello, G. K. James, I. Kanik and B. O. Franklin, *J. Geophys. Res.*, 1992, **97**, 10473.
54 J. Schneider, R. Pflieger, S. Nikitenko, S. Schukin and H. Mohwald, *J. Phys. Chem. A*, 2011, **115**, 136.
55 NIST Atomic Spectra Database Lines Form.
56 R. S. Schappe, M. B. Schulman, F. A. Sharpton and C. C. Lin, *Phys. Rev. A*, 1988, **38**, 4537.
57 S. D. Hopkins, S. J. Putterman, B. A. Kappus, K. S. Suslick and C. G. Camara, *Phys. Rev. Lett.*, 2005, **95**, 254301.
58 G. H. Dieke and H. M. Crosswhite, *J. Quant. Spectrosc. Radiat. Transfer*, 1961, **2**, 97.
59 G. N. Chapman and A. J. Walton, *J. Appl. Phys.*, 1983, **54**, 5961.
60 M. Virot, T. Chave, S. I. Nikitenko, D. G. Shchukin, T. Zemb and H. Mohwald, *J. Phys. Chem. C*, 2010, **114**, 13083.